International Journal of Minerals, Metallurgy and Materials
Volume 26, Number 5, May 2019, Page 657
https://doi.org/10.1007/s12613-019-1774-0

Study on the thermal deformation behavior and microstructure of FGH96 heat extrusion alloy during two-pass hot deformation

Bin Fang[1)], *Gao-feng Tian*[2)], *Zhen Ji*[1)], *Meng-ya Wang*[1)], *Cheng-chang Jia*[1)], *and Shan-wu Yang*[1)]

1) School of Materials Science and Engineering, University of Science and Technology Beijing, Beijing 100083, China

2) Beijing Institute of Aeronautical Materials, Beijing 100095, China

(Received: 14 July 2018; revised: 15 October 2018; accepted: 19 October 2018)

Abstract: The change rules associated with hot deformation of FGH96 alloy were investigated by isothermal two-pass hot deformation tests in the temperature range 1050–1125°C and at strain rates ranging from 0.001 to 0.1 s^{-1} on a Gleeble 3500 thermo-simulation machine. The results showed that the softening degree of the alloy between passes decreases with increasing temperature and decreasing strain rates. The critical strain of the first-pass is greater than that of the second-pass. The true stress–true strain curves showed that single-peak dynamic recrystallization, multi- peak dynamic recrystallization, and dynamic response occur when the strain rate is 0.1, 0.01, and 0.001 s^{-1}, respectively. The alloy contains three different grain structures after hot deformation: partially recrystallized tissue, completely fine recrystallized tissue, coarse-grained grains. The small-angle grain boundaries increase with increasing temperature. Increasing strain rates cause the small-angle grain boundaries to first increase and then decrease.

Keywords: FGH96 super-alloy; two-pass hot deformation; microstructure; grain orientation

1. Introduction

FGH96 alloy is one of the Ni-based superalloys. It is the preferred material for aero-engine turbine disks because of its uniform microstructure, fine grain size, and good fatigue properties [1–2].

Two forming processes are used with FGH96 alloy: hot isostatic pressing and heat extrusion. The hot isostatic pressing process has been intensively studied. Powder particle boundary (PPB) formation in the microstructure is a known problem. The γ′ phase, MC carbides, and oxides constitute the PPB. It causes cracking, which adversely affects the material strength and plasticity [3–4]. Research has shown that the γ′ phase can be reduced to the nanometric scale via heat extrusion and heat treatment while the PPB is simultaneously dispelled [5].

The present research mainly focuses on one-pass hot deformation [6–9], which tends to lead to fracture of the alloy because of excessive strain. Turbine disks are usually produced through two- or three-pass hot deformation. Some scholars have studied the hot deformation and processing map of the hot isostatic pressed FGH96 superalloy [10–12].

In the present work, we investigated two-pass hot deformation of heat-extrusion FGH96 superalloy using a Gleeble 3500 thermo-simulation machine. The hot deformation was investigated in the temperature range from 1050 to 1125°C and at a strain rate from 0.001 to 0.1 s^{-1} with 20% + 50% deformation. Using this approach, we deduced effective parameters for the hot deformation of this alloy.

2. Experimental

The components of the alloy are listed in Table 1. The strain rates were 0.1, 0.01, and 0.001 s^{-1}; meanwhile, the deformation temperatures were 1050, 1075, 1100, and 1125°C. The strain of two-pass hot deformation was 20% + 50%, as determined from research related the different deformation strains. The materials required a large strain de-

Corresponding author: Zhen Ji E-mail: jizhen@mater.ustb.edu.cn

formation, almost 70% deformation strain, for forging. One-pass deformation was found to break down the alloy; it therefore needed two or passes for deformation. In addition, lower first-pass deformation has been shown to result in a reduction of cracks in the alloy [12]; specifically, 30% deformation causes few cracks [12] and 20% deformation strain may be better. The critical strain for dynamic recrystallization for the components of this alloy is less than 0.2 [10]. The duration of the two passes was 8 s. Samples were cooled with water immediately after deformation to maintain the microstructure pattern of high-temperature deformation. The microstructure of hot extruded samples and hot deformation samples were observed by optical microscopy. The microstructure was observed using an optical microscope and a chemical etchant of $CuCl_2$ (10 g) + HCl (50 mL) + H_2O (50 mL). The grain orientation of hot deformation samples was analyzed by electron-backscatter diffraction (EBSD).

Table 1. Chemical composition of the FGH96 superalloy wt%

Ni	Cr	Co	Mo	Al	Ti	W	Nb	C	B	Zr
55.68	15.78	13.04	4.33	4.14	3.88	2.26	0.82	0.03	0.01	0.03

3. Results and discussion

3.1. The microstructure of alloy before hot deformation

PPB is easily observed in Ni-based superalloys prepared through hot isostatic pressing. However, Fig. 1(a) shows no PPB in the superalloy prepared in the present work because shear action refined the γ′ phase to nanometer dimensions through heat extrusion. Fig. 1(a) also shows that the grain size was small. The average size was 1.38 μm, and the microstructure was composed of equiaxed crystals. Fig. 1(b) shows that the small-angle grain boundary ratio was small. The proportion of 60° grain boundaries was particularly high, indicating that the ratio of crystal twins was large.

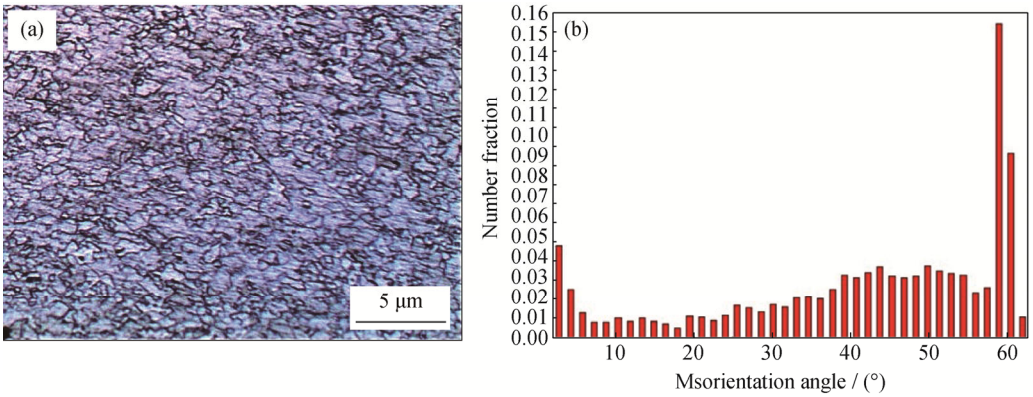

Fig. 1. Metallographic morphology (a) and orientation difference distribution (b) of hot extruded FGH96 superalloy.

3.2. True stress–true strain curves

The microstructure evolution during hot deformation was complex. The temperature, strain rate, and duration of the two phases all influence the superalloy microstructure. Fig. 2 shows the true stress–true strain curves of the FGH96 superalloy. The stress at the beginning of the second-pass deformation was smaller than the stress at the end of the first-pass deformation; however, it was higher than the stress value of the first-pass plastic deformation. These results are attributed to a large number of dislocations being produced in the alloy during the first-pass hot deformation and the dislocation twisting into a cell-like structure and then undergoing sub dynamic recrystallization, static recovery, and static recrystallization during the deformation time of the two phases. Other scholars have reported that the softening fraction substantially increases with increasing pre-strain, strain rate, and deformation temperature [13].

The driving force of these three factors originated from the energy stored during the process of thermal deformation. The nuclei of sub dynamic recrystallization formed during the process of thermal deformation; thus, the alloy directly entered the process of sub dynamic recrystallization at the end of the first-pass deformation and did not need to undergo the process of nucleation and inoculation. The static recovery process was similar to the sub dynamic recrystallization process: the static recovery began at the end of the first-pass deformation, but the softening effect of the static recovery on the alloy was weak.

Static recrystallization included two processes: nucleation and growth. Because the nucleation required a certain period of inoculation, the static recrystallization occurred later. There was a stronger softening effect on the alloy. The degree of stress softening after two-pass deformation (the difference between the stress value of the end of first-pass and that at the second initial plastic deformation) increased with

increasing strain rate at the same deformation temperature. The static recrystallization increased under the driving pressure resulting from the reduction of stored energy and grain-boundary energy [14].

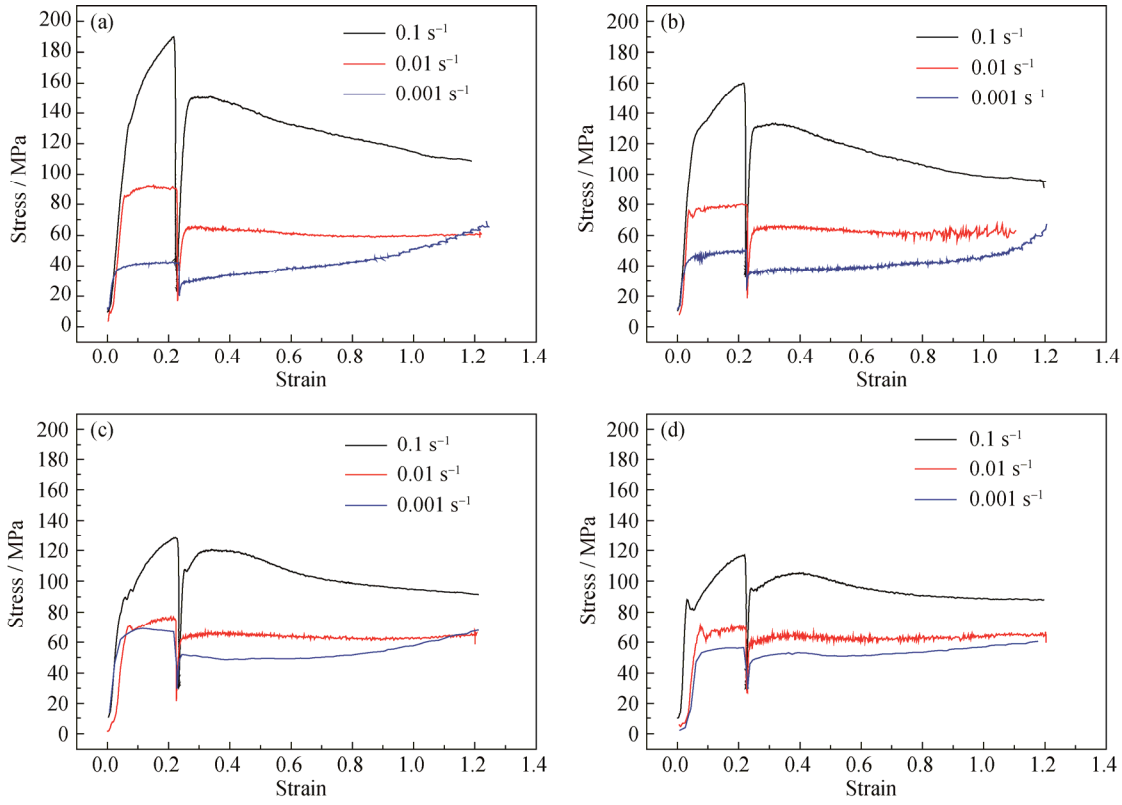

Fig. 2. True stress–strain curves for different thermo-deformation regimes: (a) 1050°C; (b) 1075°C; (c) 1100°C; (d) 1125°C.

Fig. 2(a) shows that the stress softening degree at a strain rate of 0.1 s^{-1} was much higher than that at a strain rate of 0.001 s^{-1} under the same deformation conditions. This greater stress softening degree is attributed to the high-temperature deformation of the alloy, which was sensitive to the transmission rate; when the strain rate was higher, the stored energy could not be released during the deformation process. Therefore, the stored deformation energy could be released during the heat preservation of the pass, thus decreasing the subsequent deformation stress.

At the same time, the thermal insulation period was too short to completely eliminate work hardening; thus, the stress of initial plastic deformation was higher. The critical recrystallization strain of the second-pass was obviously lower than that of the first-pass under the same deformation conditions. This effect was also attributed to the insulation period between passes not completely eliminating work hardening. The second critical recrystallization strain increased with increasing deformation temperature, indicating that higher temperatures led to more extensive recrystallization.

The alloy exhibited different changes at different strain rates. At 0.1 s^{-1}, the curve showed a single peak, whereas the curve was multi modal at 0.01 s^{-1} and no obvious peak occurred at 0.001 s^{-1}. Because the recrystallization rate was slow at the 0.1 s^{-1} deformation rate, the second round of recrystallization began before the first round of recrystallization was completed; thus, the stress–strain curve consistently showed a partial recrystallization and the curve was smooth. At 0.01 s^{-1}, the second round of recrystallization began after the first round of recrystallization, and the process was repeated; the resultant stress–strain curves were multimodal. When the deformation condition was 0.001 s^{-1}, the alloy mainly recovered.

Fig. 2 shows that the alloy obviously yielded at high temperatures. In the curve obtained at 1050°C and 0.1 s^{-1}, the first stage of the plastic deformation stage did not exhibit yield points; however, in the curve obtained at 1125°C and 0.1 s^{-1}, yield points appeared in the first stage of the plastic deformation. These yield points were related to the pinning dislocation of the Cottrell air mass. At lower temperatures, the γ′ phase in the alloy did not dissolve into the matrix. At higher temperatures, the γ′ phase completely dissolved into the matrix to form a solid solution and the solute atoms in-

teracted with the dislocations to form solute atoms. Dislocation movements required moving out of the Cottrell air pinning under a larger force, which formed the upper yield point. The movement of the dislocations was easier after they were free; thus, the stress decreased and the lower yield points appeared. Therefore, the high-temperature stress–strain curves show the yield phenomena.

The stress–strain curve shows that creep was similar to that of the superalloy at low strain rates. The similar creep gradually became less obvious with increasing deformation temperature, and the same creep was most significant at 1050°C and 0.001 s^{-1}. Some scholars have also found that, with different strain rates in two-pass deformation, the true stress of the second-pass distinctly increases [15].

3.3. Microstructure of alloy after hot deformation

The deformation temperature, rate, strain, and number of deformation passes were all found to be important factors affecting the thermal deformation of the alloy. The deformation temperature and deformation rate strongly influence the grain size in the final tissue. With increasing deformation temperature and decreasing deformation rate, the grain size after dynamic recrystallization increased gradually. High temperatures increased the growth rate of recrystallized grains, whereas low rates were beneficial to the dynamic recovery of dislocations and were not conducive to recrystallization nucleation. Therefore, low temperatures and high speeds were favorable conditions for obtaining fine-grained structures. He *et al*. [13] noted that the metadynamic recrystallization grain size sharply increased when the pre-strain and deformation temperature were increased and obviously decreased with increasing strain rate.

The metallographic structure of the samples with two-pass (20% + 50%) deformation and different deformation parameters is shown in Fig. 3. A dynamic recrystallization process clearly occurred during the deformation process. The alloy mainly exhibited three grain morphologies: partially recrystallized grains, complete fine recrystallized grains, and coarse grains.

A large number of non recrystallized structures were observed in the sample deformed at 1050°C and 0.1 s^{-1}. The large amount of γ′ phase at this temperature strongly inhibited recrystallization. With decreasing deformation rate, the increase of the non recrystallization volume in the alloy (i.e., the dynamic recrystallization volume fraction) increased with increasing strain rate. Other authors have reported an increase of the dynamic recrystallization volume fraction with decreasing strain rate of a Ni-based superalloy [16]. In the structure composed of distorted grains, aggregation recrystallization was achieved through grain-boundary migration in the subsequent heat-treatment process. Because of the influence of the deformation energy and the preferred orientation of the morphed tissue, the grain size was difficult to control and the mixed crystal structure was easily formed. In addition, the recrystallized grains in the microstructure recrystallized at this temperature were smaller than those of samples deformed at other temperatures. This smaller grain size reason was not only due to low temperatures, which made the grain boundary migration rate low, but also due to the existence of the γ′ phase and the pinned grain boundary, which made growth of the grain difficult.

As shown in Figs. 3(d), 3(e), 3(h) and 3(g), as the amount of γ′ phase decreased, almost all the alloys underwent dynamic recrystallization. Their grains also grew to a certain extent when the deformation temperature was 1075–1100°C and the deformation rate was 0.1–0.01 s^{-1}. At this time, although the γ′ phase was not completely dissolved, complete recrystallization occurred, mainly because the strain promoted dynamic recrystallization and induced recrystallization nucleation. This microstructure was beneficial to obtaining a uniform grain size during the subsequent heat treatment; thus, the thermal deformation under these conditions was favorable for attaining the ideal deformation structure.

As shown in Figs. 3(j)–3(l), when the alloy was deformed at 1125°C, at which the γ′ phase completely dissolved, the microstructure was completely recrystallized and the grain was coarse. The occurrence of this coarse recrystallized structure was related to the complete dissolution of the γ′ phase at the beginning of deformation and increased the initial grain size. As the original grain size increased, the original grain boundary area was reduced, so the preferential recrystallization nucleation zone was reduced, which led to a decrease of the nucleation rate. The growth rate of recrystallized grains increased with increasing temperature. The results also showed that coarse grains and dissolution of the γ′ phase were enhanced with increasing deformation temperature [15].

In addition, Fig. 3 shows that the uniformity of the deformable tissue was strongly affected by the deformation temperature and that the microstructure uniformity of the specimen differed dramatically at different temperatures. When the deformation condition was 1050°C and 0.1 s^{-1}, the microstructure of the specimen was obviously free-forging non uniform. The non uniform microstructure of the alloy deformed at 1075°C and 0.01 s^{-1} was improved. The recrystallized grains grew, which may be related to the nucleation mode of the alloy under different deformation

conditions. At low rates, such as thermal deformation at 1050°C and 0.1 s^{-1}, the dynamic recrystallization and sub crystalline coarsening mechanism coexist with the strain-induced mechanism, where the strain-induced dynamic recrystallization was the dominant mechanism. By contrast, at high rate, the sub crystalline coarsening mechanism becomes the dominant mechanism, such as in the case of thermal deformation at 1075°C and 0.01 s^{-1}.

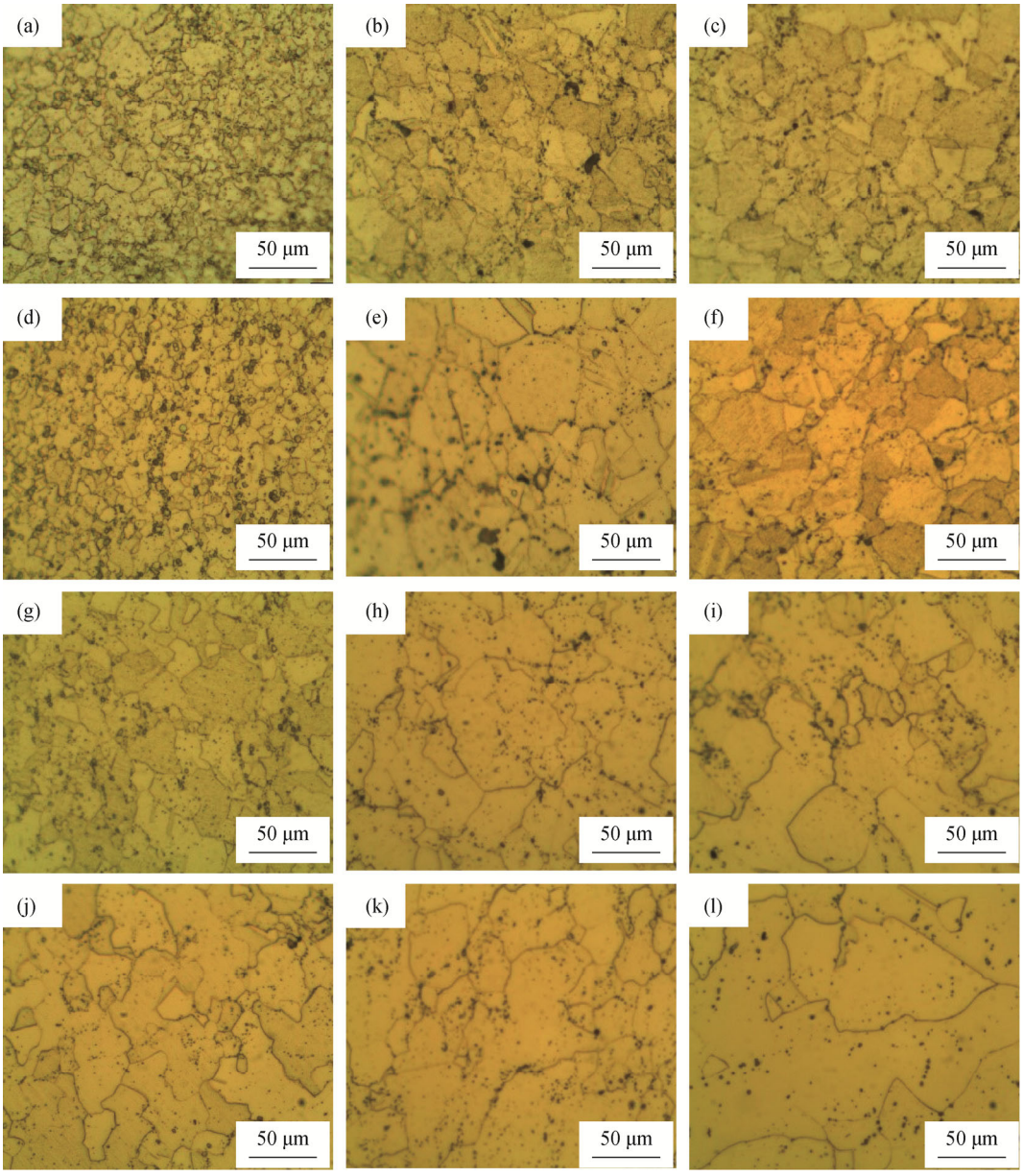

Fig. 3. Metallographic morphology after double-pass (20% + 50%) deformation with different deformation parameters: (a) 1050°C, 0.1 s^{-1}; (b) 1050°C, 0.01 s^{-1}; (c) 1050°C, 0.001 s^{-1}; (d) 1075°C, 0.1 s^{-1}; (e) 1075°C, 0.01 s^{-1}; (f) 1075°C, 0.001 s^{-1}; (g) 1100°C, 0.1 s^{-1}; (h) 1100°C, 0.01 s^{-1}; (i) 1100°C, 0.001 s^{-1}; (j) 1125°C, 0.1 s^{-1}; (k) 1125°C, 0.01 s^{-1}; (l) 1125°C, 0.001 s^{-1}.

Under the two investigated deformation temperatures, an increase of strain was beneficial to dynamic recrystallization nucleation.

3.4. EBSD analysis

Fig. 4 shows that the small-angle grain boundary ratio in the alloy deformed at 0.1 s^{-1} and 0.001 s^{-1} increased with increasing deformation temperature; by contrast, in the alloy deformed at 0.01 s^{-1}, the grain orientation of the sample first increased and then decreased under different thermal deformation conditions. This different was attributed mainly to the recrystallized grain size of the alloy increasing with increasing deformation temperature and to the number of grain boundaries of the alloy decreasing. At the same time,

with increasing temperature, the γ′ phase in the alloy gradually dissolved in the matrix and became the solute atoms. Thus, the solute atoms hindered dislocation slip and climbing, thereby hindering the migration of grain boundaries. Thus, the ratio of the sub grain boundary in the recrystallized and non recrystallized alloys increased. When the alloy was deformed at 1125°C and 0.01 s^{-1}, the curve showed several inflection points because of the alternating evolution of recrystallization and hardening. The sample was likely obtained from the recrystallization stage of the alloy. The proportion of the sub grain boundary in the alloy was very small.

The small-angle grain boundary first increased and then decreased with decreasing deformation rate. This behavior might be related to the recrystallization nucleation mode of the alloy. The growth of the alloy was mainly in the form of sub grain growth when the deformation rate was 0.1 s^{-1}. The alloy nucleation point was increased and the recrystallization rate was higher. When the alloy was deformed at 0.01 s^{-1} and 0.001 s^{-1}, the alloy exhibited strain-induced grain-boundary migration, which resulted in relatively fewer nuclei and slowed the elimination of dislocations and sub crystals. When the deformation rate was 0.01 s^{-1}, the sub grain boundary ratio was higher. When the deformation rate was 0.001 s^{-1}, the transition nucleation of the strain-induced crystal boundary occurred, but the deformation time was sufficient. The sub crystal had sufficient time to complete recrystallization, resulting in a low nucleation ratio.

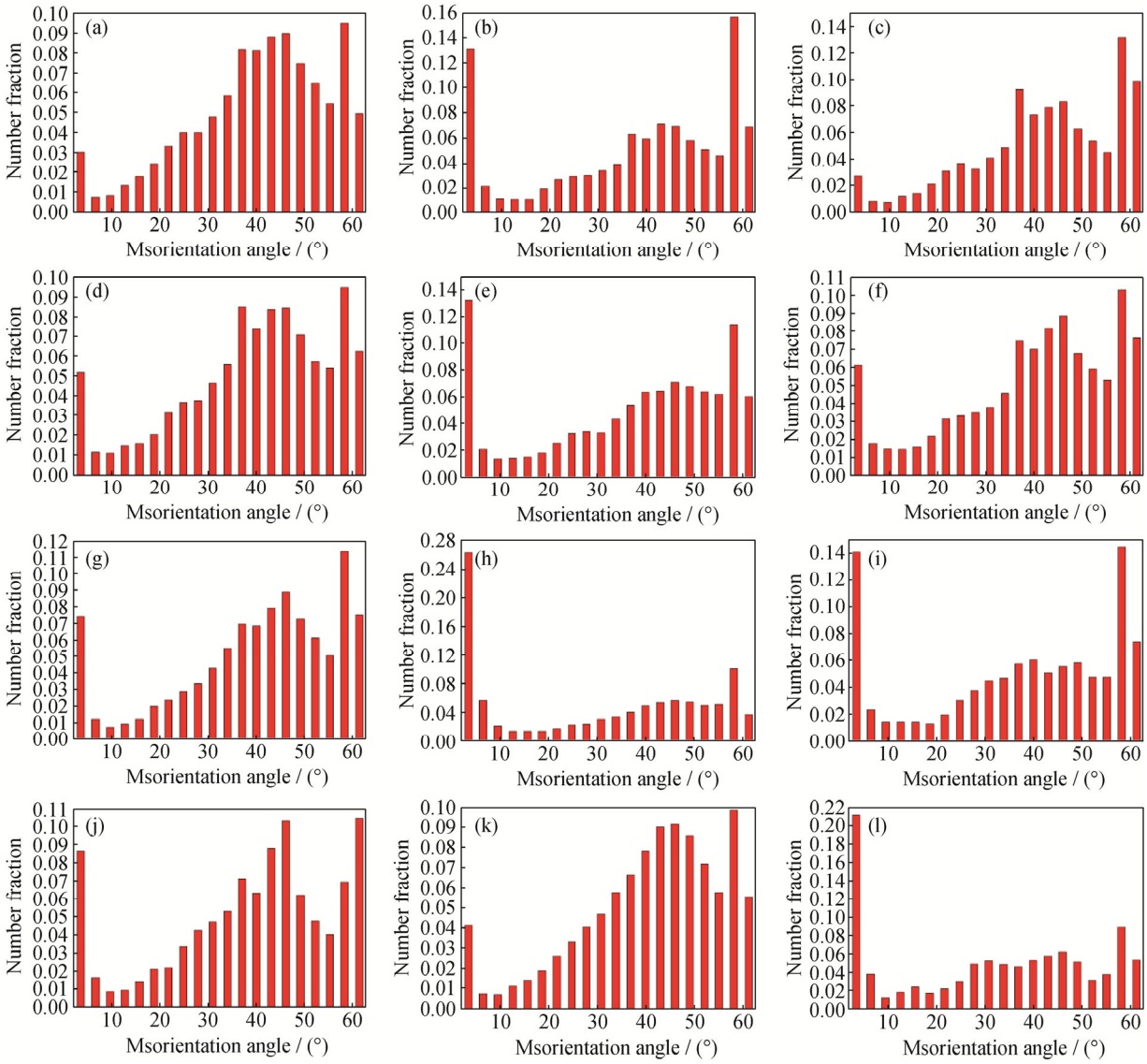

Fig. 4. Difference in grain orientation under different thermal deformation conditions: (a) 1050°C, 0.1 s^{-1}; (b) 1050°C, 0.01 s^{-1}; (c) 1050°C, 0.001 s^{-1}; (d) 1075°C, 0.1 s^{-1};(e) 1075°C, 0.01 s^{-1}; (f) 1075°C, 0.001 s^{-1}; (g) 1100°C, 0.1 s^{-1}; (h) 1100°C, 0.01 s^{-1}; (i) 1100°C, 0.001 s^{-1}; (j) 1125°C, 0.1 s^{-1}; (k) 1125°C, 0.01 s^{-1}; (l) 1125°C, 0.001 s^{-1}.

4. Conclusions

In this paper, hot deformation experiments of hot extruded FGH96 alloy on a Gleeble-3500 thermal simulator were conducted. Our conclusions are summarized as follows:

(1) The recrystallization softening of the alloy occurs in the deformation gap, and the softening degree decreases with increasing temperature and decreasing deformation rate.

(2) The recrystallization and softening behaviors of the alloy under different deformation conditions.

(3) The alloy mainly consists of three different structures after deformation: partially recrystallized, completely fine recrystallized, and coarse-grained structures.

(4) The small-angle grain boundary in the alloy increases with increasing deformation temperature. The small-angle grain boundary of the alloy first increases and then decreases with decreasing deformation rate.

Acknowledgement

Financial support from the National Natural Science Foundation of China (No. 51471023) and the Ministry of Science and Technology of the People's Republic of China (National 973 Program, No. 2014GB120000) are gratefully acknowledged.

References

[1] S.L. Semiatin, J.M. Shank, A.R. Shiveley, W.M. Saurber, E.F. Gaussa, and A.L. Pilchak, The effect of forging variables on the supersolvus heat-treatment response of powder-metallurgy nickel-base superalloys, *Metall. Mater. Trans. A.*, 45(2014), No. 13, p. 6231.

[2] J. Li and H.M. Wang, Microstructure and mechanical properties of rapid directionally solidified Ni-base superalloy Rene41 by laser melting deposition manufacturing, *Mater. Sci. Eng. A*, 527(2010), No. 18-19, p. 4823.

[3] M.J. Zhang, F.G. Li, S.Y. Wang, and C.Y. Liu, Effect of powder preparation technology on the hot deformation behavior of HIPed P/M Nickel-base superalloy FGH96, *Mater. Sci. Eng. A*, 528(2011), No. 12, p. 4030.

[4] M.J. Zhang, F.G. Li, Z.W. Yuan, J. Li, and S.Y. Wang, Effect of heat treatment on the micro-indentation behavior of powder metallurgy nickel based superalloy FGH96, *Mater. Des.*, 49(2013), p. 705.

[5] C.Z. Liu, F. Liu, H. Lan, and L. Jiang, Effect of hot extrusion and heat treatment on microstructure of nickel-base superalloy, *Trans. Nonferrous Met. Soc. China*, 24(2014), No. 8, p. 2544.

[6] X.H. Xie, Z.K. Yao, Y.Q. Ning, H.Z. Guo, Y. Tao, and Y.W. Zhang, Dynamic recrystallization and grain refining of superalloy FGH4096, *J. Aeronaut. Mater.*, 31(2011), No. 1, p. 20.

[7] Z.H. Yao, J.X. Dong, and M.C. Zhang, Microstructure control and prediction of GH738 superalloy during hot deformation I. Construction of microstructure evolution model, *Acta Metall. Sin.*, 47(2011), p. 1581.

[8] P.F. Liu, D. Liu, Z.J. Luo, W.R. Sun, S.R. Guo, and Z.Q. Hu, Flow behavior and dynamic recrystallization model for GH761 superalloy during hot deformation, *Rare Met. Mater. Eng.*, 38(2009), No. 2, p. 275.

[9] Z.G. Wu, D.F. Li, S.L. Guo, Q.M. Guo, and H.J. Peng, Dynamic recrystallization models of GH625 Ni-based superalloy, *Rare. Met. Mater. Eng.*, 41(2012), p. 235.

[10] B. Fang, Z. Ji, M. Liu, G.F. Tian, C.C. Jia, T.T. Zeng, B.F. Hu, and Y.H. Chang, Critical strain and models of dynamic recrystallization for FGH96 superalloy during two-pass hot deformation, *Mater. Sci. Eng. A*, 593(2014), p. 8.

[11] B. Fang, Z. Ji, M. Liu, G.F. Tian, C.C. Jia, T.T. Zeng, B.F. Hu, and C.C. Wang, Study on constitutive relationships and processing maps for FGH96 alloy during two-pass hot deformation, *Mater. Sci. Eng. A*, 590(2014), p. 255.

[12] B. Fang, Z. Ji, G.F. Tian, C.C. Jia, B.F. Hu, and Z.W. Cui, Flow behavior and processing map of FGH96 superalloy during two-pass hot deformation, *Chin. J. Eng.*, 37(2015), No. 3, p. 336.

[13] D.G. He, Y.C. Lin, M.S. Chen, and L. Ling, Kinetics equations and microstructural evolution during metadynamic recrystallization in a nickel-based superalloy with δ phase, *J. Alloys Compd.*, 690(2017), p. 971.

[14] Y.C. Lin, Y.X. Liu, M.S. Chen, M.H. Huang, X. Ma, and Z.L. Long, Study of static recrystallization behavior in hot deformed Ni-based superalloy using cellular automaton model, *Mater. Des.*, 99(2016), p. 107.

[15] D.G. He, Y.C. Lin, J. Chen, D.D. Chen, J. Huang, Y. Tang, and M.S. Chen, Microstructural evolution and support vector regression model for an aged Ni-based superalloy during two-stage hot forming with stepped strain rates, *Mater. Des.*, 154(2018), p. 51.

[16] Y.C. Lin, F. Wu, Q.W. Wang, D.D. Chen, and S.K. Singh, Microstructural evolution of a Ni–Fe–Cr-base superalloy during non-isothermal two-stage hot deformation, *Vacuum.*, 151(2018), p. 283.